1-1-2013

Demonstration of tunable optical delay lines based on apodized grating waveguides

Saeed Khan
University of Central Florida

Sasan Fathpour
University of Central Florida

Demonstration of tunable optical delay lines based on apodized grating waveguides

Saeed Khan[1,2] and Sasan Fathpour[1,2,*]

[1]*CREOL, The College of Optics and Photonics, University of Central Florida, Orlando, FL 32816 USA*
[2]*Department of Electrical Engineering and Computer Science, University of Central Florida, Orlando, FL 32816 USA*
[*]*fathpour@creol.ucf.edu*

Abstract: High-speed and tunable integrated optical delay lines are demonstrated based on silicon grating waveguides apodized by the super-Gaussian function. The submicron channel waveguides with inward-apodized gratings are fabricated by deep-ultraviolet optical lithography. Characterization of the compact delay lines shows that they offer true-time delays as long as 132 ps, tuning range of ~86 ps, and a minimum bit rate of ~13 Gb/s. For lower bit rates, delays as high as 220 ps and tuning range of 174 ps are feasible.

OCIS codes: (250.0250) Optoelectronics; (250.5300) Photonic integrated circuit.

References and links

1. S. Fathpour and N. A. Riza, "Silicon-photonics-based wideband radar beamforming: basic design," SPIE J. Optical Eng. **49**(1), 018201 (2010).
2. Y. Okawachi, M. A. Foster, X. Chen, A. C. Turner-Foster, R. Salem, M. Lipson, C. Xu, and A. L. Gaeta, "Large tunable delays using parametric mixing and phase conjugation in Si nanowaveguides," Opt. Express **16**(14), 10349–10357 (2008).
3. E. Choi, J. Na, S. Ryu, G. Mudhana, and B. Lee, "All-fiber variable optical delay line for applications in optical coherence tomography: feasibility study for a novel delay line," Opt. Express **13**(4), 1334–1345 (2005).
4. S. Yegnanarayanan, P. D. Trinh, F. Coppinger, and B. Jalali, "Compact silicon-based integrated optic time delays," IEEE Photon. Technol. Lett. **9**(5), 634–635 (1997).
5. F. Xia, L. Sekaric, and Y. Yurii, "Ultracompact optical buffers on a silicon chip," Nat. Photonics **1**(1), 65–71 (2007).
6. A. Melloni, A. Canciamilla, C. Ferrari, F. Morichetti, L. O'Faolain, T. F. Krauss, R. De La Rue, A. Samarelli, and M. Sorel, "Tunable delay lines in silicon photonics: coupled resonators and photonic crystals, a comparison," IEEE Photon. J. **2**(2), 181–194 (2010).
7. Q. Li, A. A. Eftekhar, P. Alipour, A. H. Atabaki, S. Yegnanarayanan, and A. Adibi, "Low-loss microdisk-based delay lines for narrowband optical filters," IEEE Photon. Technol. Lett. **24**(15), 1276–1278 (2012).
8. P. A. Morton, J. Cardenas, J. B. Khurgin, and M. Lipson, "Fast thermal switching of wideband optical delay line with no long-term transient," IEEE Photon. Technol. Lett. **24**(6), 512–514 (2012).
9. Y. Jiang, W. Jiang, X. Chen, L. Gu, B. Howley, and R. T. Chen, "Nano-photonic crystal waveguides for ultra-compact tunable true time delay lines," Proc. SPIE **5733**, 166–175 (2005).
10. J. Adachi, N. Ishikura, H. Sasaki, and T. Baba, "Wide range tuning of slow light pulse in SOI photonic crystal coupled waveguide via folded chirping," IEEE J. Sel. Top. Quantum Electron. **16**(1), 192–199 (2010).
11. S. Khan, M. A. Baghban, and S. Fathpour, "Electronically tunable silicon photonic delay lines," Opt. Express **19**(12), 11780–11785 (2011).
12. S. Khan and S. Fathpour, "Complementary apodized grating waveguides for tunable optical delay lines," Opt. Express **20**(18), 19859–19867 (2012).
13. Y. A. Vlasov, M. O'Boyle, H. F. Hamann, and S. J. McNab, "Active control of slow light on a chip with photonic crystal waveguides," Nature **438**(7064), 65–69 (2005).
14. Y. A. Vlasov and S. J. McNab, "Coupling into the slow light mode in slab-type photonic crystal waveguides," Opt. Lett. **31**(1), 50–52 (2006).
15. G. P. Agrawal, *Fiber-optic Communication Systems* (Wiley, 2002), p. 26.
16. I. Giuntoni, D. Stolarek, D. I. Kroushkov, J. Bruns, L. Zimmermann, B. Tillack, and K. Petermann, "Continuously tunable delay line based on SOI tapered Bragg gratings," Opt. Express **20**(10), 11241–11246 (2012).

1. Introduction

Tunable optical delay lines are essential devices for a variety of photonic system applications, including optical beam-forming for controlling phased-array antennas (PAAs) [1], optical

#192685 - $15.00 USD Received 21 Jun 2013; revised 28 Jul 2013; accepted 2 Aug 2013; published 12 Aug 2013

communication networks [2] and optical coherence tomography [3]. In particular, integrated true-time delay lines on silicon have been pursued since 1997 [4]. Coupled-resonator optical waveguides (CROW) [5,6], over-coupled microdisk resonators [7], side-coupled integrated spaced sequence of resonators (SCISSOR) [8] and photonic crystal (PhC) line-defect waveguides [6, 9, 10] are more recent demonstrated device architectures.

We have recently proposed a novel class of tunable photonic delay lines based on apodized gratings [11,12]. Our architecture offers a compromised solution between size, loss and speed of operation. That is, the proposed devices may not be as compact as other mentioned approaches, but it was predicted that they attain comparable insertion losses and can operate at bit rates as high as 100 Gb/s [12]. Transmission and reflection modes of operation can be envisaged and the performance can be enhanced by cascading the devices. Electrooptic [11] or thermooptic [12] effects can be utilized to tune the true-time delay of the devices. In this paper, this previously proposed approach is experimentally demonstrated and the fabricated optical delay lines are characterized in the transmission mode and compared with theory.

2. Operating principle and design

Figure 1(a) shows the schematic of an inward apodized grating waveguide photonic delay line for transmission mode of operation. Multiple reflections in the distributed Bragg reflectors slow down the light and lead to enhanced delay for the transmitting signal (see Fig. 1(b)). By keeping the incident wavelength fixed, and by increasing the refractive index via the thermooptic effect, the whole delay spectrum of the device can be red-shifted. As a result, the delay in the transmitted light will decrease due to anomalous dispersion of the inward grating in the delay spectrum at the operating wavelength. Apodized gratings need to be used, rather than uniform gratings, as follows. Easy and efficient apodization of grating waveguides, as compared with PhC or ring-resonator-based devices, allows significantly reducing the interface reflection of the gratings with input/output waveguides and hence avoiding group delay ripples that arise in uniform grating devices in the vicinity of the operating wavelength. Another advantage is that the devices do not suffer from interface reflection losses, as discussed below. The fabricated devices consist of silicon-on-insulator (SOI) waveguides with inward grating profiles apodized by the super-Gaussian function [12]. Super-Gaussian apodization is preferred to linear, Gaussian or raised cosine profiles, as it offers more compact tapered regions.

The delay lines were designed and optimized by calculating transmission coefficients of the structures using the standard transfer matrix method [11,12]. The effective refractive index of each corrugated section was determined by utilizing the commercial simulation software COMSOL™.

According to our optimized designs, for single-mode waveguides at operating wavelengths around 1550 nm, the fabricated grating waveguide needs to have a width W of 580 nm, a grating length L of 2.5 mm, a maximum grating width w of 65 nm and a grating period Λ of 330 nm [Fig. 1(a)]. The full width at half maximum (FWHM) of the employed super-Gaussian apodization function of order 12 is 1.75 mm. SOI wafers with a 220-nm-thick silicon layer on a 2-μm-thick buried oxide layer are used to achieve channel-shaped grating waveguides. It is noted that these submicron waveguide cross-sections are much smaller than our previous designs [11,12].

Delay tuning was achieved by using the thermooptic effect via microheaters fabricated on top of grating waveguides. An increase in temperature of silicon causes an increase of the material refractive index, resulting in a red shift of the whole delay spectrum of the device. As the dispersion of the delay spectrum is anomalous in the vicinity of the operating wavelength in inward apodized gratings, the signal delay decreases by temperature increase, provided that the signal wavelength is fixed at the highest value of its range.

#192685 - $15.00 USD Received 21 Jun 2013; revised 28 Jul 2013; accepted 2 Aug 2013; published 12 Aug 2013

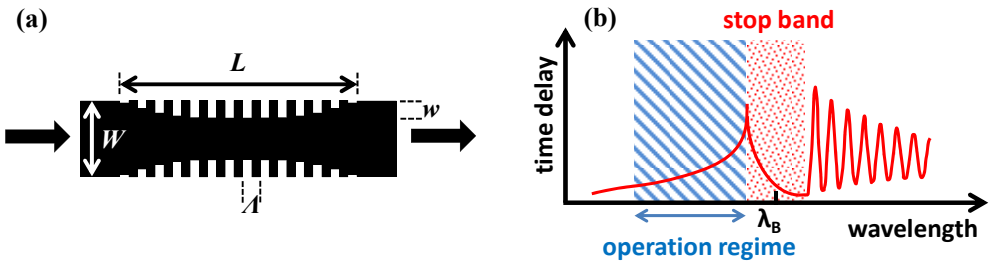

Fig. 1. Schematic of (a) the fabricated inward apodized grating waveguide photonic delay line, (b) the delay spectrum showing the wavelength operating regime.

3. Experimental results

The designed grating waveguides were fabricated in the frame of ePIXfab setup by IMEC vzw CEA using a complementary metal–oxide–semiconductor (CMOS)-compatible process using 193-nm deep ultraviolet (UV) lithography. The microheaters are made of 2-μm-wide, 110-nm-thick Ti/TiN metallic layers. A 600-nm-thick SiO_2 layer isolates the Ti/TiN layer from the silicon grating waveguide to minimize the optical loss. Grating fiber couplers are used at each end of the devices to launch the transverse-electric (TE) optical power of a laser source in and out of the chip via single-mode optical fibers. The grating period of the fiber coupler is 630 nm, which is designed for maximum efficiency at ~1550 nm wavelength. The grating fiber couplers are 20 μm long, 10 μm wide and the corrugation depth is 70 nm.

Single-grating, delay lines (case A) were fabricated and their transmission spectra were measured (the red line in Fig. 2(a)). These are the real devices for practical delay line applications that can, in principle, be characterized by real-time pulsed measurements utilizing a network analyzer [4]. However, it is perhaps more convenient to integrate them in Mach–Zehnder interferometer (MZI) configuration and study their phase properties, from which the actual time delay can be extracted [13]. In the MZI devices (case B in Fig. 2(a)), the reference arm contain similar grating waveguides but with longer periods of 335 nm. The longer-grating device in the reference arm is used to balance the loss of the arms. Meanwhile, the 5-nm larger grating period red-shifts its band-edge wavelength by ~10 nm (according to Fig. 2), giving an almost flat reference delay, corresponding to its propagation length. A larger delay in the signal arm, compared to the reference arm of the MZI, results in interference fringes in the transmission spectrum of the MZI (the longer the delay, the faster the fringe oscillation). Hence, using the wavelengths of maxima and minima of the MZI fringes, λ_{max} and λ_{min}, the delay of the signal arm can be conveniently calculated using $T_{sig} = \lambda_{\max}\lambda_{\min}/[2c(\lambda_{\max} - \lambda_{\min})] + T_{ref}$, where c is the speed of light in vacuum and T_{ref} is the delay of the reference arm.

The blue line in Fig. 2(a) shows the transmission spectrum of a typical MZI at 0 V of bias, while the green line shows the transmission spectrum when 15 V is applied to the integrated microheater. To exclude the losses of fiber couplers and MZI from the loss calculations of the delay line, an MZI without any gratings was also fabricated on the same die. The black line in Fig. 2(a) shows the transmission spectrum from this device (case C).

Figure 3 shows the delay versus wavelength, extracted from the wavelength location of the minima and maxima of the grating waveguide in the MZI configuration (device B), for 0 V (blue triangles) and 15 V (red circles) biases. The solid lines show the simulation fittings to the results, based on the model described elsewhere [11,12]. Here, the waveguide width W and maximum grating width w are varied to fit the experimental data, using the least squares method. The fitted values used for simulations in Fig. 3 are W = 570 nm and w = 73 nm, which are somewhat different than W = 580 nm and w = 65 nm in the designed lithographic mask. The discrepancy could be due to fabrication errors or inaccurate estimation of the refractive index profiles in the simulations. The blue line in Fig. 3 is obtained by assuming

#192685 - $15.00 USD Received 21 Jun 2013; revised 28 Jul 2013; accepted 2 Aug 2013; published 12 Aug 2013

that the grating is at room temperature (R_T), while the red line was obtained by keeping W and w fixed at the above fitted values, and then adjusting the device temperature to fit the experimental data at 15 V of bias. At 15 V of applied bias, the dissipated power is ~0.5 Watt. Simulation fitting to the experimental data suggests that the waveguide temperature increases by ~20 °C for this amount of power dissipation (see Fig. 3).

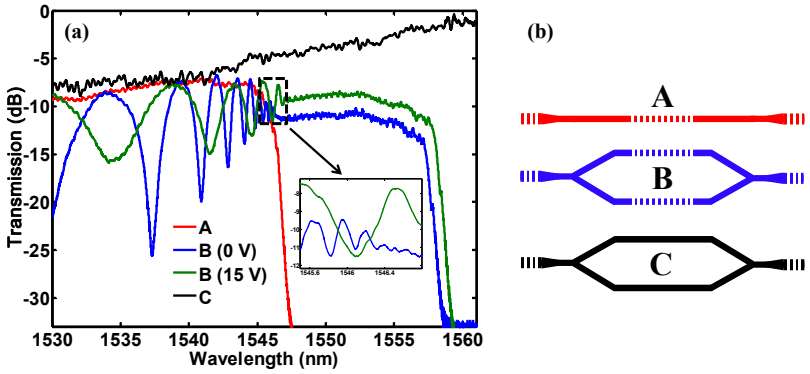

Fig. 2. (a) Transmission spectra of non-MZI grating waveguides (case A), MZI with grating at two different biases (case B), and MZI device without any gratings (case C); (b) Schematics of the three device cases in (a).

Fabrication errors also cause another discrepancy between the designed and measured values. Theoretically, the 5-nm larger grating period in the reference arm should red-shift the Bragg wavelength by ~28 nm and the 126-nm stop-band width should remain unchanged. Since measuring such a wide stop-band width was not possible by our tunable laser, it is not easy to verify these values experimentally. Nonetheless, the smaller measured shift of ~10 nm in the band-edge (according to Fig. 2) may suggest that the stop-band width could have increased by 36 nm (2 × (28 nm −10 nm) = 36 nm). A possible explanation for the bandwidth increase could be that a larger periodicity results in better-developed grating corrugation features during the development of the photoresist and the subsequent dry etching, which in turn results in higher coupling coefficient and hence higher stop-band width.

Figure 4(a) shows the insertion loss of the grating device (blue triangles) and its reflectivity (red circles) versus extracted delay values. What meant by reflectivity here is not the Bragg reflector reflectivity, as the operating wavelength is outside the stop band. Rather, the reflectivity is from the index contrast at the interface of the gratings and the input/output waveguides [14], as discussed further below.

Loss values are obtained from the maxima of the transmission spectrum of the MZI with gratings (case B in Fig. 2(a)) [13,14], after normalizing it to the transmission spectrum of the MZI without gratings (case C in the same figure). Therefore, the loss values exclude the coupling loss from the fiber couplers and the linear propagating loss of simple waveguides, but include the two components of the grating loss, i.e., scattering from the grating sidewalls and reflection of the gratings. The extracted low interface reflectivity of < 3% emphasizes that this factor is not a major contributor to the overall loss in our pass-band regime of interest. Hence, the loss values in Fig. 4(a) is attributed to the scattering loss of the gratings, which varies from 2 to 9.3 dB for delays of 27 to 220 ps. The low reflectivity values are possible here due to efficient apodization of the grating by the super-Gaussian function, unlike uniform gratings that can suffer from high reflectivities at the abrupt interfaces [14]. The reflectivity, R is calculated from $V = 2R/(1+R^2)$, where $V = (I_{max} - I_{min})/(I_{max} + I_{min})$ is the interference fringe visibility, calculated from the amplitude of maxima I_{max} and minima I_{min} in Fig. 2(a) [14].

#192685 - $15.00 USD Received 21 Jun 2013; revised 28 Jul 2013; accepted 2 Aug 2013; published 12 Aug 2013

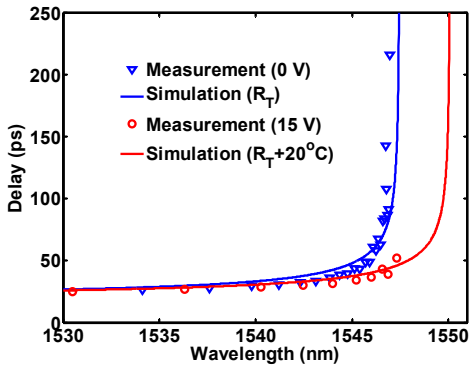

Fig. 3. Delay spectrum extracted from wavelength location of the minima and maxima from grating waveguide in MZI configuration (device B in Fig. 2) at 0 V applied bias (blue triangles) and at 15 V applied bias (red circles). Solid line shows the simulation results for the corresponding conditions. R_T = Room Temperature

Figure 4(b) shows the dispersion induced limit on the bit rate and time delay for different bias voltages, estimated from the discussed fitted simulations to the experiments, corresponding to different applied biases. The bit rate was calculated from broadening of transform-limited input pulses due to the dispersion of the delay line. The estimation criterion was that 95% of the output pulse energy would be confined to its corresponding time slot [15]. In each simulation, the grating waveguide temperature was adjusted to fit the experimental data for the corresponding bias value, using the least squares method. The input signal was assumed to be at 1547.3 nm wavelength, at which both time delay and bit rate are sufficiently large (132 ps and 13 Gb/s, respectively). Fixing the signal at longer wavelengths would offer higher delay values (see Fig. 3), but the bit rate will be reduced due to higher dispersion. For instance, 220 ps delay and a tuning range of 174 are possible if high-speed operation is not required. In contrast, lower signal wavelength will result in higher bit rate but lower delay. At the compromised wavelength choice of 1547.3 nm, by varying the applied voltage from 0 V to 15 V, the time delay varies from ~132 ps to ~46 ps. Meanwhile, the maximum limit on bit rate varies from ~13 Gb/s to ~93 Gb/s. Hence, at this particular signal wavelength, the operating bit rate is at least 13 Gb/s, the attainable tunability is ~86 ps, the tunability-bit-rate product is 1.12, and the delay-bit-rate-product is 1.72. Higher operational bit rates (up to 100 Gb/s) with tunability-bit-rate product of 2.8, and the delay-bit-rate-product of 6.1 are feasible if two apodized grating waveguides with opposite dispersion are cascaded, as we have proposed elsewhere [12]. As explained therein, this higher delay- and tunability-bit-rate products are possible because two complementary grating waveguides compensate each other's dispersions. Based on the applied mirror-imaged apodization of the cascaded grating waveguides, their dispersions are compensated such that the combined bit rate can increase by factor of about three in our particular design. Demonstration of such cascaded devices is underway.

It is noted that we have previously proposed the operation of apodized grating delay lines in the reflection mode [11]. Such reflection-mode devices were later demonstrated by I. Giuntoni *et al*. [16]. Although they use linear apodization and somewhat different waveguide designs, it may be instructive to compare the performance of our transmission-mode to their reflection-mode devices. They achieved a tunability of 450 ps for a 2-cm-long device, and an operation speed of 25 Gb/s, which could be extended to 80 Gb/s if proper dispersion compensation scheme is used. The higher tunability in their case is mostly due to a factor of 8 longer devices.

#192685 - $15.00 USD Received 21 Jun 2013; revised 28 Jul 2013; accepted 2 Aug 2013; published 12 Aug 2013

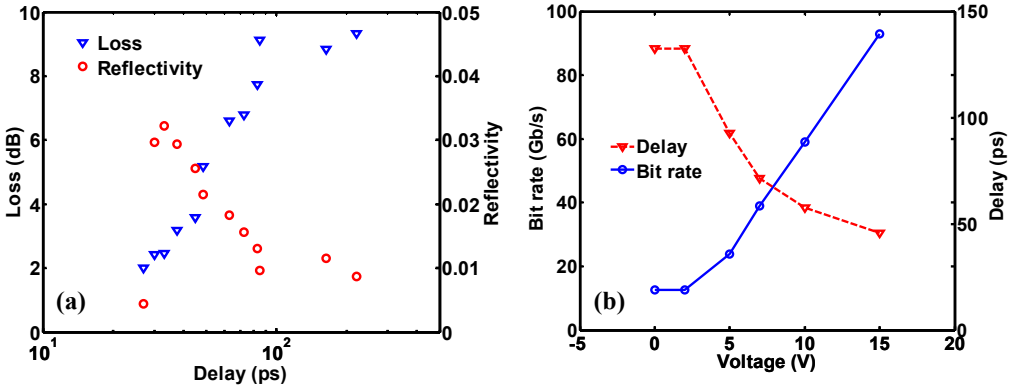

Fig. 4. (a) Loss and reflectivity from grating edges versus delay (b) Bit rate and delay versus applied bias.

4. Conclusions

In summary, optical delay lines based on apodized inward grating waveguides are demonstrated on a CMOS-compatible SOI waveguide technology. Characterization of the devices show that at a bit rate of 13 Gb/s, delay times as high as 132 ps with a tunability of 86 ps are possible via the thermooptic effect. Higher delays of 220 ps, along with a tuning range of 174 ps, are also possible in the 2.5-mm long devices, but at the expense of reduced bit rate.

Acknowledgment

The work is being supported by the United States' National Science Foundation under the Award Number 1128208.

#192685 - $15.00 USD Received 21 Jun 2013; revised 28 Jul 2013; accepted 2 Aug 2013; published 12 Aug 2013